Climatology of Normal Mode Rossby Waves

JON E. AHLQUIST

Department of Meteorology, Florida State University, Tallahassee, FL 32303

(Manuscript received 28 February 1985, in final form 20 May 1985)

ABSTRACT

Three years of twice-daily NMC global operational analyses were projected onto normal mode Rossby waves to produce a climatology of these waves. For zonal wavenumbers 1 through 4, annual average geopotential amplitudes at 50 kPa are about 5 gpm for the gravest symmetric meridional mode, and 10 and 20 gpm for the next two meridional modes, although the amplitude for a given time and latitude can greatly exceed the average. Seasonal average amplitudes differ by less than ±25% from the annual average. The modes' frequencies drift during the course of a year, but this variation is not correlated with season.

Autocorrelations of Rossby wave time series become negligible for lags greater than approximately ten days, which is of the order of the wave period.

For all ten modes examined, geopotential fluctuations exist in both Northern and Southern Hemispheres.

1. Introduction

Within a linearized approach, atmospheric normal modes are waves whose speeds and structures are determined by the resonant characteristics of the atmosphere rather than by forcing mechanisms. Madden (1979) and Salby (1984) have reviewed studies of planetary scale traveling waves, of which normal mode Rossby waves are a special case. Theoretical properties of these waves have been studied by Kasahara (1980, 1981) and Salby (1980, 1981a,b), among others. Daley (1981) has reviewed the use of normal modes to initialize numerical models. Ahlquist (1982) identified twelve normal mode Rossby waves in the National Meteorological Center (NMC) operational global analyses. Lindzen *et al.* (1984) have studied the behavior of nine Rossby modes during 1979 using global analyses from the European Centre for Medium Range Weather Forecasts (ECMWF).

All normal mode Rossby waves travel westward. Their tropospheric vertical structure is similar to that of a Lamb wave, i.e., negligible tilt and vertical velocity, maximum pressure changes at the surface, and geopotential disturbance and horizontal velocity proportional to p^{-R/c_p}. The effects of a nonisothermal and nonresting basic state are more prominent above the troposphere (Geisler and Dickinson, 1976; Schoeberl and Clark, 1980, and Salby, 1981a,b), and Madden and Labitzke (1981) have confirmed this observationally for one of the modes. Horizontally, the geopotential perturbations of these Rossby waves are largest in midlatitudes. We shall index a normal mode Rossby wave by (s, l), where s is the zonal wavenumber and l is the meridional mode number, defined as the number of nodes in the meridional velocity profile between the north and south poles. [Some authors use the index (s, n), where $n = s + l$.] The latitude of maximum geopotential response and the wave period are both monotonic increasing functions of the meridional mode l, and vary weakly with zonal wavenumber s.

Daley *et al.* (1981) have shown that planetary scale normal mode Rossby waves are excited excessively in some numerical models, causing noticeable errors after as little as 24 hours of model integration. In fact, (Daley *et al.*, 1981, p. 1845), suppression of selected normal mode Rossby waves can improve hemispheric forecasts more than suppression of gravity waves when crude tropical initial conditions are specified. Even with proper tropical initial conditions, hemispheric forecasts are contaminated by overly strong normal Rossby waves. Roads and Somerville (1982) also have confirmed this. Daley *et al.* (1981) note in their conclusion that proper treatment of normal mode Rossby waves in numerical models is difficult because the waves' atmospheric climatologies are largely unknown.

The present study seeks to fulfill this request for normal mode climatologies by a more thorough analysis of the observed normal mode time series derived by Ahlquist (1982). Section 2 presents histograms of observed normal mode amplitudes. Section 3 discusses interseasonal variability of Rossby mode amplitude and frequency. Section 4 uses autocorrelations to examine the coherence time of normal mode Rossby waves. Section 5 looks at the correlation between normal mode Rossby waves and Northern and Southern Hemisphere geopotential fluctuations. Results are summarized in Section 6.

2. Histograms of normal mode amplitudes

Ahlquist (1982) projected 1200 days of twice daily operational global analyses produced by the National Meteorological Center (NMC) onto the planetary scale normal mode Rossby waves of classical Laplace tidal theory. This resulted in a time series of amplitude and phase for each mode studied. This projection process may be outlined as follows. For each analysis time, the NMC global analyses for geopotential height h, and horizontal wind velocity, u and v, at 85, 50, and 20 kPa were Fourier analyzed in longitude at each 10° of latitude between 80°N and 80°S. The Lamb mode structure, p^{-R/c_p}, was then least squares fitted through the three levels for u, v, and h independently for each zonal wavenumber 1 through 4 at each latitude. Last, the amplitude and phase for each Rossby mode, (s, l), was determined by a process equivalent to least squares fitting the Lamb mode components for zonal wavenumber "s" to the (s, l) mode's meridional Hough function structure for u, v, and h. See Ahlquist (1982, hereafter A82) for more information.

We have reanalyzed ten of A82 time series to estimate the typical distribution of normal mode amplitudes in the NMC global analyses. These ten barotropic modes are the $l = 1$ to 3 modes detected by A82. Their approximate frequencies are shown in Table 1. These frequencies are the peak frequencies in the spectra of Fig. 4 of A82. To avoid seasonal bias in this study, we trimmed A82 twice daily time series to an integral number of years, three to be exact, running from 1 September 1976 through 31 August 1979.

Each time series was then bandpass filtered by Fourier transforming, zeroing out the average and all coefficients for frequencies that were more than ±0.05 cycles day^{-1} from the appropriate frequency in Table 1, and inverse transforming. This bandwidth spans all the normal mode peaks in Fig. 4 of A82. Even with this filtering, each $l = 3$ time series is contaminated by low frequencies not directly associated with the normal mode (see Fig. 4 of A82), but the contamination was not judged to be severe because the $l = 3$ filtered time series behaved similarly to the $l = 1$ and $l = 2$ time series.

TABLE 1. Frequencies (in cycles day^{-1}) of normal mode Rossby waves as determined observationally from the spectral peaks in Fig. 4 of Ahlquist (1982). Negative frequencies indicate westward motion.

	l		
s	1	2	3
1	−0.21	−0.10	−0.05
2	−0.24	−0.125	−0.05
3	−0.22	−0.11	—
4	−0.17	−0.09	—

Figure 1 shows the resulting wave amplitudes at 50 kPa sorted according to their frequency of occurrence to form histograms. (e.g., see Jenkins and Watts, 1968, p. 64.) The histograms are scaled so that they may be interpreted as probability density functions. That is, the integral of such a function from one amplitude to another is the probability (the fraction of time) that the amplitude lies in that amplitude range. For meridional modes 1, 2, and 3, the average amplitudes at 50 kPa are about 5, 10, and 20 gpm, respectively. A mode's maximum amplitude during the three year period is roughly three times its average amplitude, and the standard deviation is about 50% of the average amplitude. The amplitudes in Fig. 1 apply to the latitude where the geopotential portion of a mode's Hough function is a maximum. This varies between 30° and 65° latitude, depending on the meridional mode l. (See A82, Fig. 1.)

The amplitudes of this study are less than those reported by Madden (1978) and Hirooka and Hirota (1985), who did not constrain a wave's global structure. For example, during solstice periods, the Northern and Southern Hemispheres exhibit an uncorrelated response for the (1, 3) mode, with the winter hemisphere response being much larger. Daley and Williamson (1985) demonstrated that the (1, 3) mode (or something like it) existed in only the Northern Hemisphere during January 1979. We shall return to this matter in Section 5. Thus, at any given time, the time series of the present study generally overestimate the wave amplitude in one hemisphere and underestimate it in the other hemisphere. These time series have two benefits, however. One, the present time series are stationary and so are candidates for standard statistical analysis. (This matter is discussed in Section 3, where stationarity is necessary to estimate the the autocorrelations.) Two, the same projection process has been used by Lindzen *et al.* (1984) and Daley *et al.* (1981), which facilitates comparison of results. We now turn to these latter two studies.

Lindzen *et al.* (1984) used ECMWF global analyses for 1979 to study Rossby mode behavior at 50 kPa. To minimally constrain their time series, they filtered their time series to retain all disturbances that move westward faster than the frequency of the annual cycle. This means that their time series for any given normal mode included frequencies not directly associated with that mode, so it is not surprising that Lindzen *et al.*'s maximum amplitude (see their table 3 in conjunction with their Fig. 2) are somewhat larger than those shown in Fig. 1 of this study.

To more closely compare our time series with those of Lindzen *et al.*, we plotted a number of amplitude and phase records with filtering of our NMC time series similar to that done by Lindzen *et al.* In Fig. 2, we show the (3, 1) time series for May through July 1979, which can be compared to plots of the (3, 1) time series

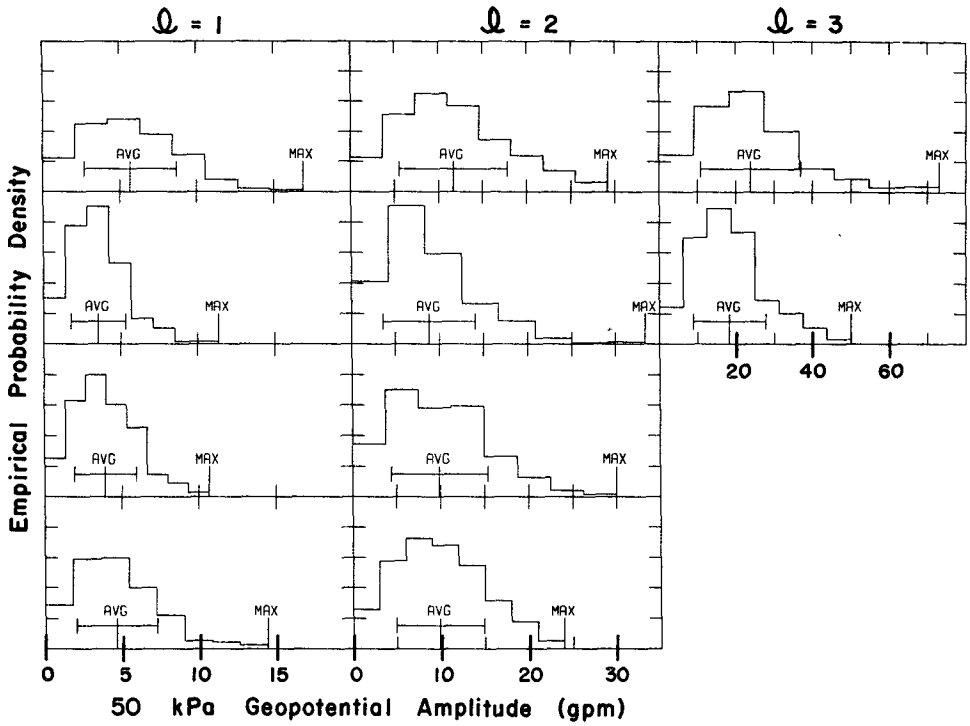

FIG. 1. Histograms of Rossby mode geopotential amplitudes at 50 kPa for the period September 1976 through August 1979. The columns are labeled with the meridional mode number l, and the rows apply to zonal wavenumbers 1–4, from top to bottom. The histograms are normalized with units of a probability density function. For l = 1, 2, and 3, the ordinate units are 0.05, 0.02, and 0.01 $(gpm)^{-1}$ per tic mark. The horizontal bar surrounding each average (AVG) denotes plus and minus one standard deviation.

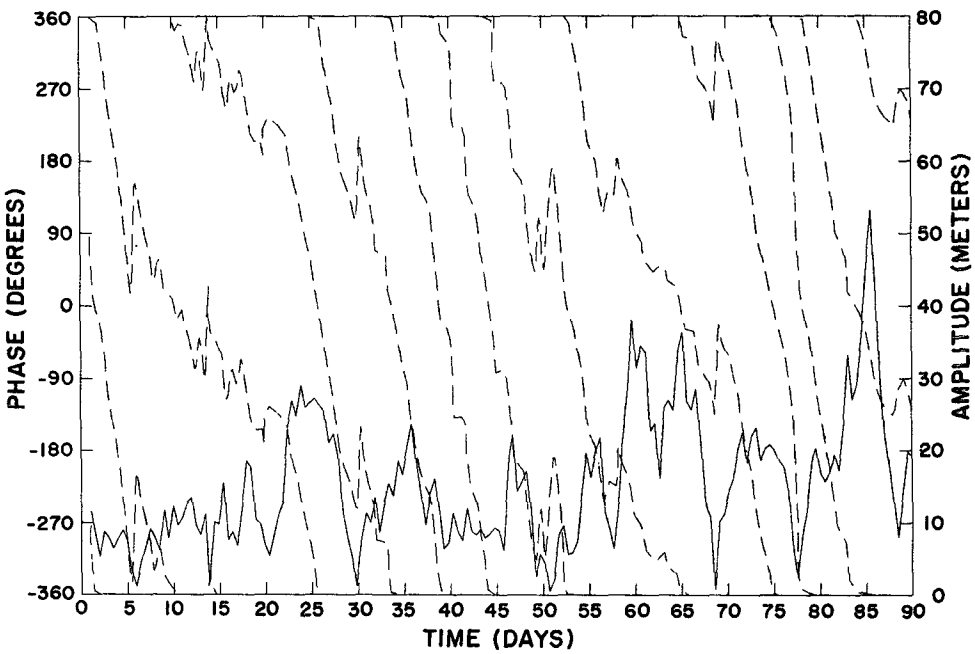

FIG. 2. Amplitude and phase of the (3, 1) mode in the NMC analyses for 90 days beginning on 1 May 1979. Ahlquist's (1982) time series for this mode was filtered to pass westward moving disturbances with periods of 50 days or less. The amplitudes are scaled for direct comparison with Fig. 9a and 9b in Lindzen *et al.* (1984). To convert these amplitudes to the mode's 50 kPa amplitude at 35° latitude, the latitude at which the mode's geopotential response is maximum, multiply these amplitudes by 0.45.

for the same time period in Lindzen *et al.*'s Fig. 9a, based on ECMWF analyses, and Fig. 9b, based on Goddard Laboratory for Atmospheric Sciences (GLAS) analyses. This comparison shows that the NMC time series is noisier than the ECMWF time series and is less noisy than the GLAS time series. Close similarities in amplitude and phase are apparent among all three analyses. The similarity is even more marked when we realize that the time series in Fig. 2 is based on data from three levels (85, 50, and 20 kPa) while Lindzen *et al.*'s time series utilized only 50 kPa data. This comparison supports statements of A82 and Lindzen *et al.* to the effect that the gross behavior of normal mode time series seems to be nearly independent of the method by which any reasonably careful global analysis is produced.

Table 2 shows the maximum amplitudes from the present study referenced to a common latitude, 40°N, instead of the latitudes of maximum Hough mode response. We can compare these amplitudes to the Rossby mode amplitudes at 50 kPa and 40°N reported by Daley *et al.* (1981, hereafter D81) in their study of planetary scale errors of several numerical models. The amplitudes from D81 models are shown in Table 3. Although D81 performed their tests using a spectral shallow water model instead of a baroclinic model, they first verified that (D81, p. 1841) "the barotropic model does a very creditable job of reproducing the long-wave errors of the barotropic component of the baroclinic model."

Comparison of Tables 2 and 3a reveals that D81 hemispheric model with artificial tropical initial conditions (model CE, in their notation) suffered from normal modes which were much stronger than the maximum amplitudes observed in the atmosphere by the author or by Lindzen *et al.* (1984). The D81 global model with proper tropical initial conditions (model CHB/G, in their notation) produced much more realistic amplitudes except for the (1, 3) mode. Thus, as D81 suggest in their introduction, part of the failure of even global models to perform well at planetary scales may be due to overly strong normal mode Rossby waves.

TABLE 3a. Amplitudes in meters of Rossby mode geopotential fluctuations at 50 kPa and 40°N produced by a five day integration of a hemispheric barotropic model with artificial tropical initial conditions. This is Daley *et al.* (1981) "CE" case; amplitudes were read from their Fig. 13. The $l = 2$ modes are all zero because of the hemispheric model's equatorial boundary conditions.

	l		
s	1	2	3
1	60	0	125
2	35	0	—
3	25	0	—

Hayashi (1981, Fig. 2) has reported realistic amplitudes for the (1, 1) and (1, 3) modes at 51.5 kPa at 40°N in a 9-layer GFDL spectral model (cf. Madden, 1978, Fig. 9). Thus, not every global model appears to suffer from overly strong normal mode Rossby waves.

3. Interseasonal variability

Madden and Stokes (1975) and Madden (1978) examined the seasonal detectability of the (1, 1) and (1, 3) modes using cross spectra. They showed that the waves' signal-to-noise ratios at midlatitudes are different in different seasons. In the Northern Hemisphere, (Madden, 1978, Figs. 1 and 2), the (1, 1) mode is most easily detected during summer, while the (1, 3) mode is most easily detected during winter. Both modes are detectable throughout the year with at least some statistical significance. Lindzen *et al.* (1984) demonstrated that the globally averaged amplitude of Rossby modes varied weakly with season during 1979. Hirooka and Hirota (1985) and Daley and Williamson (1985) have established that large differences in amplitude can exist between the Northern and Southern hemispheres during the course of the year.

With the latter caveat in mind, we have examined the interseasonal variability of the same ten modes studied in Section 1. This was done by plotting amplitude histograms of the bandpass filtered time series for each three-month season, September–October–

TABLE 2. Maximum amplitudes in meters of Rossby mode geopotential fluctuations at 50 kPa and 40° latitude during three years of twice daily NMC global analyses (September 1976 through August 1979) using the time series of Ahlquist (1982).

	l		
s	1	2	3
1	17	21	16
2	11	29	23
3	10	29	
4	13	24	

TABLE 3b. As in Table 3a, except that tropical initial conditions were generated by Cressman's method of objective analysis. This is Daley *et al.* (1981) "CHB" case; amplitudes were read from their Fig. 13 (or 18). The $l = 2$ modes are all zero because of the hemispheric model's equatorial boundary conditions.

	l		
s	1	2	3
1	30	0	125
2	20	0	—
3	15	0	—

TABLE 3c. As in Table 3a, except that the model is global and tropical initial conditions were generated by Cressman's method of objective analysis. This is Daley *et al.* (1981) "CHB/G" case; amplitudes were read from their Figs. 18 and 19.

	l		
s	1	2	3
1	10	—	60
2	10	25	—
3	5	10	—

November (SON), December–January–February (DJF), March–April–May (MAM), and June–July–August (JJA), during the three year period 1 September 1976 through 31 August 1979, where the same seasons for different years were lumped together. Seasonal histograms for the $l = 1$ modes are shown in Fig. 3. The averge amplitude is a weak function of season. Indeed, the average for any season lies within plus or minus one standard deviation of the average for any other season. Seasonal histograms for $l = 2$ and 3 behaved similarly.

Figure 4 shows the ratio of the seasonal mean to the annual mean as a function of season for all ten modes. December through February is the strongest season for six of the ten modes, while March through May is next in prominence. All the modes are weaker than average during June through August. The (1, 3) and (3, 2) modes exhibit the strongest seasonal variation in amplitude, amounting to ±25% of their annual averages.

The variability of normal mode frequencies can be seen through complex demodulation (e.g., see Bloomfield, 1976). Complex demodulation removes a carrier frequency from a time series by multiplying it by $\exp(i\omega t)$ for some frequency ω; for a complex-valued time series, this removes a linear trend in phase. In the present case, this corresponds to watching a wave from a reference frame rotating around the earth where we chose the angular velocity to be the wave's average angular velocity. For economy of presentation, only the complex demodulated record for the (1, 3) mode is displayed in Fig. 5, since the other modes behaved similarly. In detail, Fig. 5 was constructed as follows. After the bandpass filtering of Section 2, the phase time series was computed and adjusted objectively by adding multiples of 2π so that the difference in phase from one time to the next was never more than π. A line was then fitted to the phase time series using the least squared error criterion. The slope of this line was −0.046 cycles per day, and this linear trend was then subtracted from the phase time series.

The presence of phase drifts in Fig. 5 shows that the wave does not circulate steadily around the earth at the demodulating frequency. Rather, a range of frequencies is involved like that described by baroclinic modeling (Salby, 1981b). It is noteworthy that no consistent seasonality is apparent in the phase drifts, also

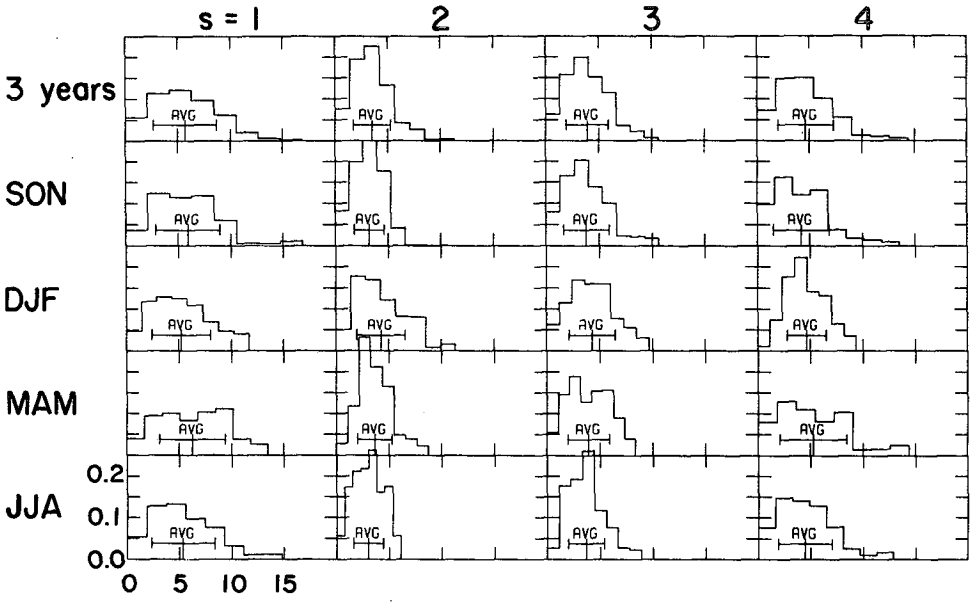

FIG. 3. Histograms showing the amplitude of the $l = 1$ Rossby modes as a function of season during September 1976 through August 1979. The top row is identical to the first column in Fig. 1 and is included for comparison. The geopotential amplitude in gpm is the abcissa and the empirical probability density in $(\text{gpm})^{-1}$, the ordinate. The labeling for the graph in the lower left corner applies to all the graphs in the figure. The horizontal bar surrounding each average (AVG) denotes plus and minus one standard deviation.

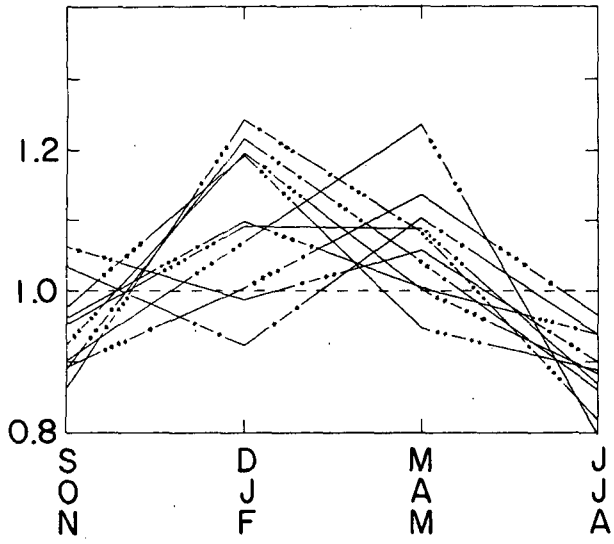

FIG. 4. Ratio of the seasonal average amplitude to the average annual amplitude for the 10 modes shown in Fig. 1. The mode number is coded into each curve by means of dot patterns. For example, the (1, 3) mode has the largest ratio during December–January–February (DJF), the (2, 1) mode the next largest, etc., with the (1, 1) mode having the smallest ratio during DJF.

in agreement with baroclinic modeling (Salby, 1981b, Fig. 4).

4. Normal-mode Rossby wave coherency times

Using observations, Madden (1983, pp. 1111–1112) estimated that the average lifetime of the (1, 3) mode is 38 days. Nonetheless, Madden was concerned that this lifetime might be an overestimate caused by overly sharp filtering. Lindzen *et al.* (1984) reported that the time scale for surges in normal mode amplitudes is on the order of 5–20 days. However, this latter figure is more a measure of how often the waves are noticeably excited than how long they survive. In this section, we estimate wave lifetime using the autocorrelation function (Morse and Ingard, 1968, pp. 54–57; Jenkins and Watts, 1968, Chapter 5).

The calculation of autocorrelations requires that a process be statistically stationary, and Salby (1980) has pointed out that normal mode behavior may be nonstationary, so this matter must be addressed first. According to Jenkins and Watts (1968, pp. 147–149), a minimum requirement for stationarity is time independence of the probability density function. The results in Section 3 show that the probability density functions for Hough mode behavior are essentially independent of season. Last, calculations (not shown) verify that the probability density functions for the first half of the three year period are like those of the second half of the three year period. Therefore, we conclude that the time series are at least minimally stationary.

Prior to the autocorrelation calculations, we filtered Ahlquist's (1982) time series with a boxcar filter centered on each mode's eigenfrequency from Table 1. Various filter widths were tried. As long as the filter width was at least 0.1 cycles day^{-1}, which was the filter width used in Section 2, results differed somewhat in detail but not in substance. For the results that will be displayed here, the filter width was 0.15 cycles day^{-1}, with the exception that the upper cutoff frequency for the two $l = 3$ modes was reduced so that the annual cycle was just excluded. After filtering, the autocovariance was estimated according to the formula

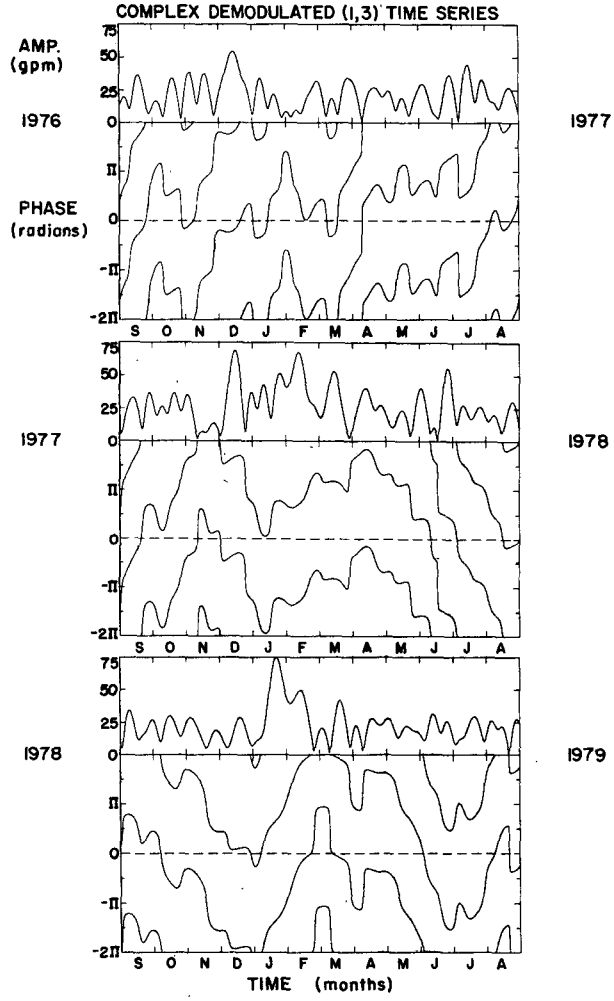

FIG. 5. Amplitude and complex demodulated phase in radians of the (1, 3) mode's geopotential fluctuations at 50 kPa and 65° latitude during September 1976 through August 1979. The latitude of maximum response is 65° for the (1, 3) mode in Laplace tidal theory. The time axes are labeled with the first letter of each month of the year beginning with September. The time series was formed by projecting the NMC global analyses onto the (1, 3) mode of Laplace tidal theory and then filtering to retain only westward propagating disturbances with frequencies between 0.001 and 0.1 cycles day^{-1}. The phase was complex demodulated by subtracting the linear trend in phase (i.e., the integrated average propagation speed).

$$C(t') = N^{-1} \sum_{t=1}^{N-t'} \text{conj}[w(t)]\, w(t + t')$$

where t' is the lag, N is the number of observations, "conj" is the complex conjugate, and $w(t)$ is the filtered version of complex-valued time series $W(t)$ representing wave amplitude and phase [See Ahlquist, 1982, for the precise definition of $W(t)$.] The autocorrelation is the autocovariance divided by the variance, i.e., the autocovariance at lag zero. The autocorrelation at negative lags is equal to the conjugate of the corresponding positive lag. The phase of the autocorrelation is the average phase difference for observations differing by lag t'; the slope is the angular rate of separation.

The estimated autocorrelation functions in Fig. 6 show that the response at any given time has antecedents which can be traced 10 days (roughly one wave period) into the past and whose consequences extend an equal time into the future. As mentioned above, this result is only a weak function of the width of the bandpass filter. The $l = 1$ modes decay somewhat faster when a somewhat wider filter is used, but a bandpass of 0.15 cycles day^{-1} more than surrounds the $l = 1$ spectral peaks in Fig. 4 of Ahlquist (1982).

For the (1, 3) mode, the antecedent plus consequent coherence time is approximately 25 days. Since this is shorter than Madden's (1983) 38 day lifetime, we repeated his compositing calculations. We began by filtering the westward traveling portions of the (1, 3) time series with a boxcar filter having the same center frequency ($\frac{1}{16}$ cycles day^{-1}) and the same bandwidth (0.043 cycles day^{-1}) as the half power points in Madden's filter (see Madden, 1978, p. 1612). Then we computed a composite of the ten most prominent maxima in the filtered (1, 3) time series, excluding any maximum that lay within 30 days of a more prominent

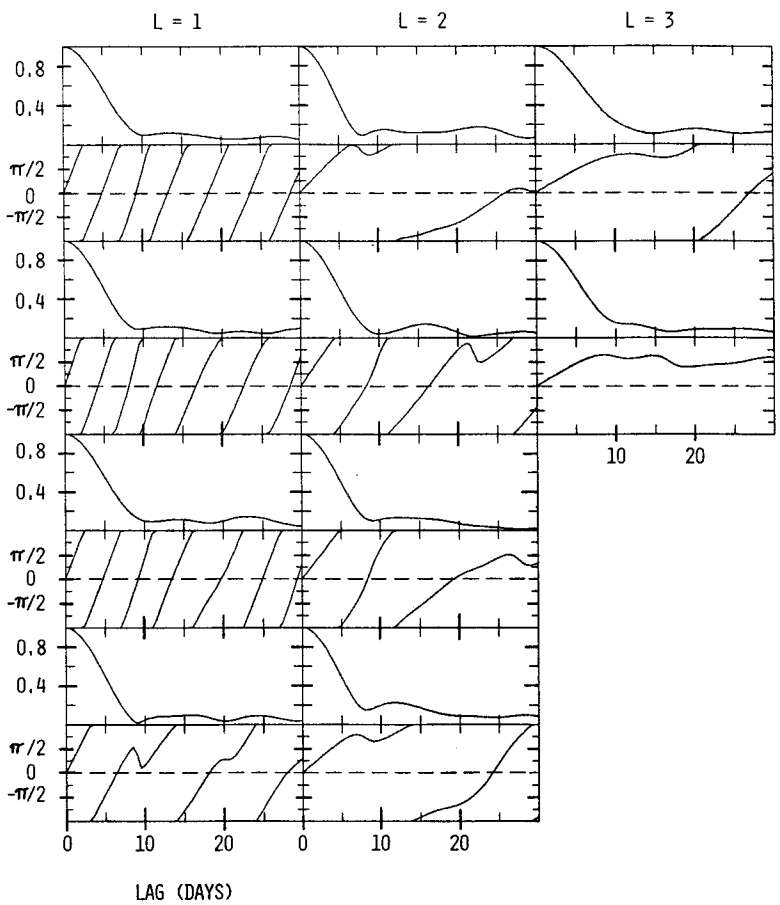

FIG. 6. Estimated autocorrelation functions (amplitude and phase) for ten Rossby modes. Before autocorrelations were estimated, each time series was filtered to retain a band of frequencies 0.15 cycles day^{-1} wide centered about the appropriate frequency from table 1. (The upper cutoff frequency for the two $l = 3$ modes was reduced so that the annual cycle was excluded.) The columns are labeled with the meridional model number l, and the rows apply to zonal wavenumbers 1–4, from top to bottom.

maximum. Before compositing, the ten segments were aligned in phase at their midpoints. The resulting composite is shown in Fig. 7a, and 40 days is indeed the lifetime that one would deduce. We then used the same ten time periods to compute a new composite, where now the time series was not filtered at all before (or after) compositing. This unfiltered composite is shown in Fig. 7b. The amplitude in Fig. 7b decays at a rate similar to that of the corresponding autocorrelation in Fig. 6. Thus, it appears that Madden (1983, p. 1112) was correct in his suggestion that his filter was too sharp. Composites (not shown) of the other modes also show amplitudes that decay at rates similar to those of their autocorrelations.

A 25 day average lifetime does not preclude incidents when the (1, 3) mode could be coherent for a notably longer interval. For example, Fig. 5 indicates that the (1, 3) mode traveled at a steady rate with significant amplitude during January and February 1979. The wave appears to have been reexcited during the first part of February. The (1, 3) mode during this period

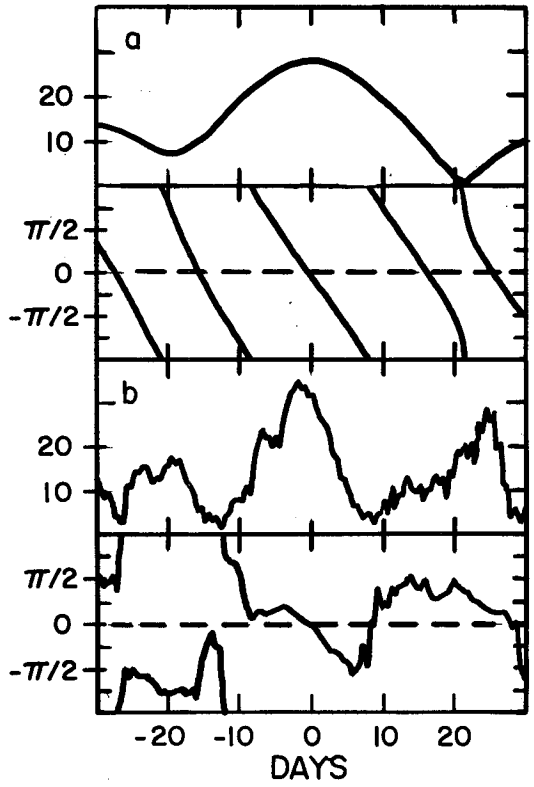

FIG. 7. Amplitude in gpm and phase in radians of composites of ten local maxima for the (1, 3) mode. In Fig. 7a, the time series was filtered before compositing to retain only westward moving fluctuations in a band centered on $^1/_{16}$ cycles day^{-1} which is 0.043 cycles day^{-1} wide. This is similar to the filtering used by Madden (1978, 1983). In Fig. 7b, the same ten periods were composited, but no filtering was applied before or after compositing.

has been investigated in detail by Madden and Labitzke (1981) and Daley and Williamson (1985).

5. Interhemispheric differences in normal mode activity

Madden and Julian (1973) showed that the (1, 1) mode is equally prominent in the Northern and Southern hemispheres. For the (1, 3) mode, Madden (1978, p. 1616) detected no statistically significant coherence between 60°N, where the (1, 3) mode is known to be strong, and 60°S, where the symmetry of this mode in Laplace tidal theory would make it equally pronounced. Schoeberl and Clark (1980), Salby (1981b), and Daley and Williamson (1985) have theoretically modeled the (1, 3) mode. Their models display interhemispheric differences during solstice conditions, but not of a magnitude to suggest that no coherence would be detected between hemispheres. During equinox conditions, the models portray normal modes as being equally strong in the Northern and Southern hemispheres. Hirooka and Hirota (1985) present an observational example from April 1979 when the (1, 3) mode was present equally in both hemispheres.

We have computed the cross spectrum between zonal wavenumber one geopotential fluctuations at 60°N and 60°S in the NMC analyses for a 1550 day data record beginning on 1 July 1976. The method of space–time spectral analysis (Hayashi, 1982) was implemented using the direct Fourier transform method. At both 50 and 20 kPa, statistically significant correlation was detected near the frequency of the (1, 1) mode but not near the frequency of the (1, 3) mode. Although this confirms Madden's (1978) findings for the (1, 3) mode, it is not consistent with the theoretical studies cited above. Therefore, we sought another test for hemispheric involvement.

What we did was to compute the coherence squared between A82 globally derived time series for each Rossby mode, (s, l), and the 50 kPa geopotential for wavenumber s at each 10° of latitude between 80°N and 80°S. In effect, this measures the extent to which the 50 kPa geopotential at a given latitude contributed to the global normal mode time series. Figure 8 shows the coherence squared. All 2400 twice daily observations in A82 time series were used for this calculation, and each spectral estimate has 128 degrees of freedom. Therefore (Bloomfield, 1976, Section 9.5), the 95% confidence limits for the coherence squared are about ±0.10.

The obvious features in Fig. 8 are (i) the high coherence at normal mode frequencies and (ii) the symmetry between the hemispheres for the l = 1 and 2 modes at their appropriate frequencies, with lesser symmetry for the l = 3 modes. The phases (not shown) associated with the squared coherences agree with the theoretical description of these waves, i.e., all latitudes

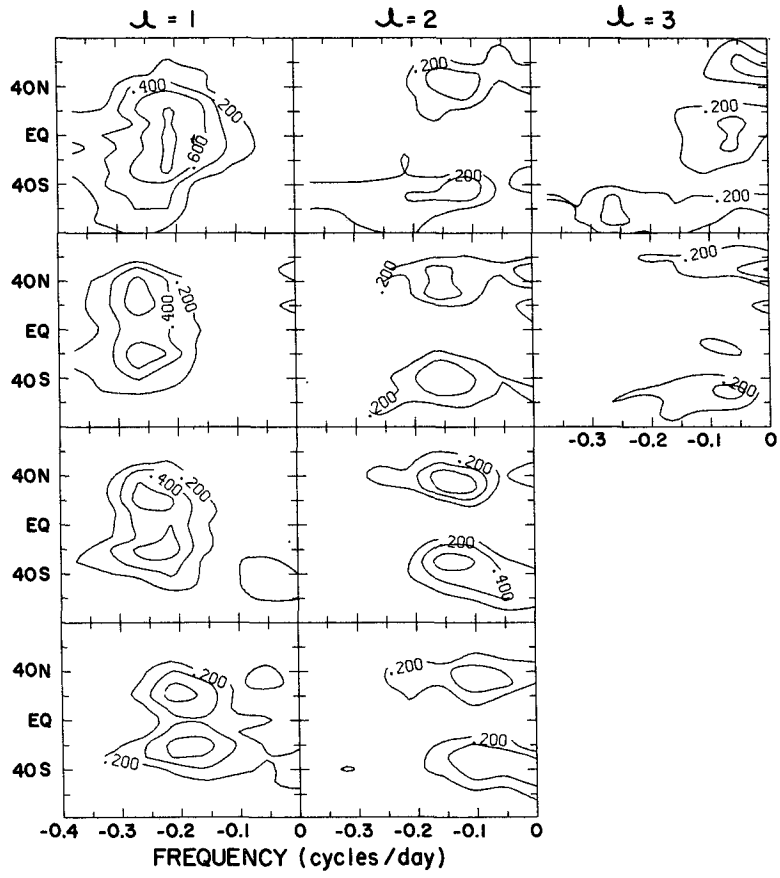

FIG. 8. Coherence squared between the time series for Rossby mode (s, l) and the 50 kPa geopotential time series for zonal wavenumber s. The columns are labeled with the meridional mode number l, and the rows apply to zonal wavenumbers 1–4, from top to bottom.

are in phase for the $l = 1$ modes, the Northern and Southern hemispheres are 180° out of phase for the $l = 2$ modes, and the subpolar latitudes of the two hemispheres are in phase for the $l = 3$ modes, with the tropics being 180° out of phase.

Apparently, the (1, 3) mode exists in both the Northern and Southern hemispheres of the NMC analyses, but without consistent correlation between the hemispheres. Hirooka and Hirota (1985) have shown that activity is concentrated in the winter hemisphere.

We also note that some of the graphs in Fig. 8 display nonzero coherence squared at frequencies other than the appropriate normal mode frequency. For example, for $s = 1$ and 2, the $l = 2$ and 3 modes exhibit squared coherencies exceeding 0.2 at Southern Hemisphere subpolar latitudes near the frequencies of the $s = 1$ modes. This is evidence that the north–south structures of the 4–5 day Rossby modes for $s = 1$ and 2 are not pure Hough functions.

6. Summary and conclusions

In the NMC global operational analyses, the annual average 50 kPa geopotential amplitudes of Rossby modes for zonal wavenumbers one through four are roughly 5 gpm for the first meridional mode, 10 gpm for the second meridional mode, and 20 gpm for the third. The maximum amplitudes for these modes in three years of NMC analyses are roughly three times the average values. These amplitudes refer to equatorially symmetric or antisymmetric structures and thereby obscure the profound hemispheric differences that can arise during solstices. Nonetheless, they confirm Daley *et al.* (1981) conclusions that deficient numerical models can excite normal modes which attain unrealistically large amplitudes.

Autocorrelations reveal that wave coherency extends approximately 10 days (order of one wave period) into the past and 10 days into the future.

We also have presented evidence that normal mode

amplitudes are not a strong function of season if the mode is considered in a global sense. This global view is justified for at least the $l = 1$ and 2 modes because both hemispheres contribute equally to the waves on an annual basis, although pronounced hemispheric differences do exist for some of the modes from season to season.

Acknowledgments. We thank D. Venne and the anonymous reviewers for suggestions which improved the manuscript. This research was supported by a grant from Florida State University and by NOAA Grant NA83AA-D-00046. The data were generated using a computer resources grant from the National Center for Atmospheric Research, which is sponsored by the National Science Foundation.

REFERENCES

Ahlquist, J. E., 1982: Normal-mode global Rossby waves: Theory and observations. *J. Atmos. Sci.*, **39,** 193–202.

Bloomfield, P., 1976: *Fourier Analysis of Time Series: An Introduction.* Wiley, 258 pp.

Daley, R. J., 1981: Normal mode initialization. *Rev. Geophys. Space Phys.*, **19,** 450–468.

——, and D. Williamson, 1985: In search of the 16 day external Rossby mode. *J. Atmos. Sci.*, **42,** 2121–2141.

——, J. Tribbia and D. Williamson, 1981: The excitation of large-scale free Rossby waves in numerical weather prediction. *Mon. Wea. Rev.*, **109,** 1836–1861.

Geisler, J. E., and R. E. Dickinson, 1976: The five-day wave with realistic zonal winds. *J. Atmos. Sci.*, **33,** 632–641.

Hayashi, Y., 1981: Space–time cross spectral analysis using the maximum entropy method. *J. Meteor. Soc. Japan,* **59,** 620–624.

——, 1982: Space–time spectral analysis and its applications to atmospheric waves. *J. Meteor. Soc. Japan,* **60,** 156–171.

Hirooka, T., and I. Hirota, 1985: Normal mode Rossby waves observed in the upper stratosphere. Part II: Second antisymmetric and symmetric modes of zonal wavenumbers 1 and 2. *J. Atmos. Sci.*, **42,** 536–548.

Jenkins, G. M., and D. G. Watts, 1968: *Spectral Analysis and its Applications.* Holden-Day, 525 pp.

Kasahara, A., 1980: Effect of zonal flows on the free oscillations of a barotropic atmosphere. *J. Atmos. Sci.*, **37,** 917–929.

——, 1981: Corrigendum. *J. Atmos. Sci.*, **38,** 2284–2285.

Lindzen, R. S., D. M. Straus and B. Katz, 1984: An observational study of large-scale atmospheric Rossby waves during FGGE. *J. Atmos. Sci.*, **41,** 1320–1335.

Madden, R. A., 1978: Further evidence of traveling planetary waves. *J. Atmos. Sci.*, **35,** 1605–1618.

——, 1979: Observations of large-scale traveling Rossby waves. *Rev. Geophys. Space Phys.*, **17,** 1935–1949.

——, 1983: The effect of the interference of traveling and stationary waves on time variations of the large-scale circulation. *J. Atmos. Sci.*, **40,** 1110–1125.

——, and P. R. Julian, 1973: Reply. *J. Atmos. Sci.*, **30,** 935–940.

——, and J. Stokes, 1975: Evidence of global-scale 5-day waves in a 73-year pressure record. *J. Atmos. Sci.*, **32,** 831–836.

——, and K. Labitzke, 1981: A free Rossby wave in the troposphere and stratosphere during January 1979. *J. Geophys. Res.*, **86,** 1247–1254.

Morse, P., and J. Ingard, 1968: *Theoretical Acoustics.* McGraw-Hill, 927 pp.

Roads, J. O., and R. C. Somerville, 1982: Predictability of ultralong waves in global and hemispheric quasi-geostrophic barotropic models. *J. Atmos. Sci.*, **39,** 745–755.

Salby, M. L., 1980: The influence of realistic dissipation on planetary normal structures. *J. Atmos. Sci.*, **37,** 2186–2199.

——, 1981a: Rossby normal modes in nonuniform background configurations. Part I: Simple fields. *J. Atmos. Sci.*, **38,** 1803–1826.

——, 1981b: Rossby normal modes in nonuniform background configurations. Part II: Equinox and solstice conditions. *J. Atmos. Sci.*, **38,** 1827–1840.

——, 1984: Survey of planetary-scale travelling waves: the state of theory and observations. *Rev. Geophys. Space Phys.*, **22,** 209–236.

Schoeberl, M. R., and J. H. E. Clark, 1980: Resonant planetary waves in a spherical atmosphere. *J. Atmos. Sci.*, **37,** 20–28.